AIP | Journal of Applied Physics

Anharmonic effects in the thermoelectric properties of PbTe

Jawaher Al-Otaibi and G. P. Srivastava

AIP | Journal of Applied Physics

Journal of Applied Physics is pleased to
announce **André Anders** as its new Editor-in-Chief

Anharmonic effects in the thermoelectric properties of PbTe

Jawaher Al-Otaibi and G. P. Srivastava
School of Physics, University of Exeter, Stocker Road, Exeter EX4 4QL, United Kingdom

In this work, we investigate the crystal anharmonic effects in the thermoelectric properties of n-type PbTe. The lattice thermal transport coefficient is computed by employing an isotropic continuum model for the dispersion relation for acoustic as well as optical phonon branches, an isotropic continuum model for crystal anharmonicity, and the single-mode relaxation time scheme. The electronic components of the transport coefficients in a wide temperature range are calculated using the isotropic-nearly-free-electron model, interaction of electrons with deformation potential of acoustic phonons, and the effect of the band non-parabolicity. It is found that the transverse optical branches play a major role in determining the phonon conductivity and the thermoelectric figure of merit of this material. © 2014 AIP Publishing LLC. [http://dx.doi.org/10.1063/1.4891201]

I. INTRODUCTION

Thermoelectric (TE) materials have been used widely in a vast variety of applications in direct heat-to-electricity converters and electronic coolers[1] with many attractive features, such as no noise and vibration. The efficiency of TE power generators is defined by a dimensionless parameter known as the figure of merit ZT, with $ZT = S^2 \sigma T / (\kappa_{el} + \kappa_{ph})$, where $S, \sigma, \kappa_{el}, \kappa_{ph}$, and T are, respectively, the Seebeck coefficient, the electronic conductivity, the electrical thermal conductivity, the lattice thermal conductivity, and T is the absolute temperature of the system.[2] The electronic thermal conductivity is further expressed as $\kappa_{el} = \kappa_{mp} + \kappa_{bp}$, with κ_{mp} and κ_{bp} as the monopolar and bipolar contributions, respectively. The figure of merit reveals that whenever the numerator is large with simultaneous reduction in thermal conductivity, the material is classified as good thermoelectric. Production of large-scale bulk materials with high ZT is the key to widespread adaptation of thermoelectric technology. Lead telluride (PbTe) alloys have been extensively studied and remain one of the best thermoelectric materials for applications in the mid-temperature range. Recent studies on p-type samples of optimised doping level reveal ZT values of approximately 1.4 at 750 K.[3,4] The thermal conductivity (κ) and the Seebeck coefficient (S) of several specimens of PbS, PbSe, and PbTe have been measured by Greig[5] in the temperature range 4–100 K. The work in Ref. 6 provides a detailed report of experimental measurements of S, electrical conductivity (σ) and κ for an n-type PbTe sample.

Most theoretical studies of the electronic components of the TE transport coefficients of semiconductors are based on the use of parabolic bands and isotropic effective mass theory. The electronic band structure of PbTe exhibits non-parabolicity. It has been reported in Refs. 7 and 8 that this effect may appear as a strong temperature dependence of effective mass and Lorentz number at relatively elevated temperatures and carrier concentrations.[7] Furthermore, the non-parabolicity may influence a change in the energy dependence of carrier relaxation time due to the increase in the density of states.[9,10]

A significant contributing factor that renders the large ZT value for PbTe is its low lattice thermal conductivity, which is $\kappa_{ph} \sim 2 \, \mathrm{W \, m^{-1} \, K^{-1}}$ at 300 K (Refs. 11–13) despite its simple rock salt structure. Detailed understanding of factors resulting in this low κ_{ph} value is lacking from the literature. Using a combination of inelastic neutron scattering measurements and first-principles computations of phonons, a strong anharmonic coupling between the transverse optical (TO) and the longitudinal acoustic (LA) phonons has been identified.[14] It has been suggested that this coupling is likely to play a central role in explaining the low thermal conductivity of PbTe. However, no theoretical formalism or numerical results are available to establish details of the role the TO phonons play in the lattice thermal conductivity and the thermoelectric figure of merit of PbTe.

In this work, we investigate the crystal anharmonic effects in the thermoelectric properties of n-type PbTe. The lattice thermal conductivity is computed in detail within the single mode relaxation time scheme, employing the isotropic continuum model for the dispersion relation for acoustic as well as optical phonon branches, and an isotropic continuum model for crystal anharmonicity. The electronic transport coefficients are computed within the isotropic-nearly-free-electron approximation, and we assume that charge carriers are mainly scattered by acoustic phonons. Moreover, the band non-parabolicity which will manifest itself directly through effective mass dependence on energy and indirectly through relaxation time is also included in this study. Our numerical work has been carried out with the material parameters relevant to the sample employed in the experimental study reported in Ref. 6.

II. THEORY

A. Lattice thermal transport coefficient

The lattice thermal conductivity κ_{ph} of PbTe is computed within the single mode relaxation time scheme by adopting an extension of the isotropic acoustic continuum approximation presented in Ref. 15. We replace the Brillouin zone of the

116, 043702-1

face centered cubic lattice for the rock salt structure by the Debye sphere of radius q_D and approximate the dispersion relations for the acoustic and optical phonons as

$$\omega_{TA} = c_{TA}q; \quad \omega_{LA} = c_{LA}q, \tag{1}$$

$$\omega_{TO} = \omega_{TO}^{min} + c_{TO}q; \tag{2}$$
$$\omega_{LO} = \omega_{LO}^{max} - c_{LO}q = \omega_{LO}^{min} + c_{LO}(q_D - q),$$

where q is the magnitude of phonon wave vector, c_s is the speed for phonons of polarisation s, ω_{TO}^{min} is the minimum frequency (at the zone centre) of the TO phonon, and for the LO phonon ω_{LO}^{max} is the maximum frequency (at the zone centre) and ω_{LO}^{min} is the minimum frequency (at the Debye sphere). The corresponding density of states expressions are

$$g_{TA}(\omega) = \frac{V_{crys}}{2\pi^2}\frac{\omega^2}{c_{TA}^3}; \quad g_{LA}(\omega) = \frac{V_{crys}}{2\pi^2}\frac{\omega^2}{c_{LA}^3} \tag{3}$$

$$g_{TO}(\omega) = \frac{V_{crys}}{2\pi^2}\frac{(\omega - \omega_{TO}^{min})^2}{c_{TO}^3} \quad (\text{for } \omega \geq \omega_{TO}^{min}) \tag{4}$$

$$g_{LO}(\omega) = \frac{V_{crys}}{2\pi^2}\frac{(\omega_{LO}^{max} - \omega)^2}{c_{LO}^3} \quad (\text{for } \omega_{LO}^{min} \leq \omega \leq \omega_{LO}^{max}), \tag{5}$$

where V_{crys} is crystal volume. The single-mode relaxation time expression for the lattice thermal conductivity is then written as

$$\kappa_{ph} = \frac{1}{3}\frac{\hbar^2}{k_B T^2 V_{crys}}\sum_s \int_{\omega_{min}}^{\omega_{max}} d\omega\, g_s(\omega)\omega^2 c_s^2 \tau_s(\omega, T)\bar{n}(\bar{n} + 1), \tag{6}$$

where $\omega_D = \bar{c}q_D$ is the Debye frequency, $\tau_s(\omega, T)$ is the frequency and temperature dependent relaxation time for a phonon of polarisation with frequency ω, the average phonon speed $\bar{c}$ is computed from $3/\bar{c}^3 = 2/c_{TA}^3 + 1/c_{LA}^3$, and $\bar{n} = 1/[\exp(\hbar\omega/k_B T) - 1]$ is the Bose-Einstein distribution function. Using Eqs. (2), we express Eq. (6) as

$$\kappa_{ph} = \frac{\hbar^2 q_D^5}{6\pi^2 k_B T^2}\sum_s^{TA,LA,TO,LO} c_s^4 \int_0^1 dx\, x^2 (\eta_s^* + x)^2 \tau_s \bar{n}(\bar{n} + 1), \tag{7}$$

where η_s^* takes the value η_s for $s = $ TA, LA, TO and the value $\eta_s + 1$ when $s = $ LO, with $\eta_s = \omega_s^{min}/c_s q_D$.

For an n-type single crystal sample of PbTe, we consider phonon scatterings from sample boundary (bs), point defects (pd), donor electrons (ep), and anharmonicity (anh). Following Matthiessen's rule, we express $\tau^{-1} = \tau_{bs}^{-1} + \tau_{pd}^{-1} + \tau_{ep}^{-1} + \tau_{anh}^{-1}$. The boundary scattering rate is simply written as $\tau_{bs} = c_s/L$, where L is an effective boundary length. The point defect scattering rate (arising from isotopic defects and unintentional impurities) is expressed as[16]

$$\tau_{pd}^{-1} = A_{pd}g(\omega)\omega^2 = B_{pd}(\omega_0 - \omega)^2\omega^2 \quad (\text{for } \omega_{min} \leq \omega \leq \omega_{max}), \tag{8}$$

where ω_0 is taken as ω_{min} for TA, LA, TO and as ω_{max} for LO phonons, and the constants A_{pd} and B_{pd} are directly related to the type and concentration of defects. As usually the nature and concentration of point defects are unknown, we treat B_{pd} as an adjustable parameter. The scattering rate for phonon-electron interaction is given by[17]

$$\tau_{ep}^{-1} = \frac{m_n^{*2}\Xi^2 k_B T}{2\pi\varrho c_{LA}\hbar^4}\left[z - \ln\left(\frac{1 + \exp(\xi - \zeta + z^2/16\xi + z/2)}{1 + \exp(\xi - \zeta + z^2/16\xi - z/2)}\right)\right], \tag{9}$$

where Ξ is the dilatational deformation potential, $z = \hbar\omega/k_B T$, and $\xi = m_n^* c_{LA}^2/2k_B T$.

We expect three-phonon processes to adequately describe anharmonic interactions. Expressions for the relaxation rates for a phonon mode $\boldsymbol{q}s$ undergoing Normal (N) and Umklapp (U) three-phonon processes of class 1 type ($\boldsymbol{q}s + \boldsymbol{q}'s' \to \boldsymbol{q}''s''$) and class 2 type ($\boldsymbol{q}s \to \boldsymbol{q}'s' + \boldsymbol{q}''s''$) have been derived in Ref. 15 when all phonons are from the acoustic branches. In materials such as PbTe, however, the TO branch is rather special as it is low-lying and quite similar to the acoustic branches except only that for $q = 0$ the frequency of such a mode does not go to zero as it does for the acoustic branches. It is therefore important to modify the formulation presented in Ref. 15 to deal with allowed three-phonon processes, including acoustic as well as optical phonons. In this work, we use Eqs. (2) and (5), and follow the procedure described in Ref. 15 to derive the following expression for the anharmonic scattering rate for a phonon mode $\boldsymbol{q}s$ (with $s = $ TA, LA, TO, LO)

$$\tau_{anh}^{-1}(x, s) = \frac{\hbar q_D^5 \gamma^2}{4\pi\rho\bar{c}^2}\sum_{s's''\varepsilon}\left[\int dx'(C\xi + D\xi' - \eta'')\{1 - \varepsilon + \varepsilon(C\xi + D\xi' - \eta'')\}\frac{\bar{n}'(\bar{n}_+'' + 1)}{(\bar{n} + 1)}\right.$$
$$\left. + \frac{1}{2}\int dx'(C\xi - D\xi' - \eta'')\{1 - \varepsilon + \varepsilon(C(\xi - D\xi' - \eta'')\}\frac{\bar{n}'\bar{n}_-''}{\bar{n}}\right]. \tag{10}$$

Here, γ is the Grüneisen constant, $x = q/q_D, x' = q'/q_D, \xi = \eta + x$ for $s = $ TA, LA, TO and $\xi = \eta + 1 - x$ when $s = $ LO, with similar notations for ξ' and ξ''. The first and second terms in Eq. (10) are contributed by class 1 and class 2 events,

respectively. The argument for the Bose-Einstein factor $\bar{n}_\pm''$ is $C\xi \pm D\xi' - \eta''$. The variable x is limited to $0 \leq x \leq 1$, and for a given x, the limits for x' are determined by satisfying the energy and momentum conservation conditions

$$\omega \pm \omega' = \omega'', \quad \boldsymbol{q} \pm \boldsymbol{q}' = \boldsymbol{q}'' + \boldsymbol{G}. \qquad (11)$$

Following previous suggestions,[15,18,19] for the assumed isotropic continuum, we take $\boldsymbol{G} = 2q_{\mathrm{D}}(\boldsymbol{x}\pm\boldsymbol{x}')/|(\boldsymbol{x}\pm\boldsymbol{x}')|$.

B. Electronic transport coefficients

Our calculations of the electronic transport coefficients assume isotropic band structure and that the relaxation time of electrons has a power function dependence on the carrier energy of the form $\tau \propto E^r$.[9,17,20] Due to the small scattering rates of impurity and polar optical phonons, we exclusively consider scattering of electrons with acoustic phonons,[21–24] and accordingly set $r = -1/2$.[9,20] The band non-parabolicity, which manifests itself directly through effective mass dependence on energy and indirectly through relaxation time, is included in the calculations. The energy dependence of effective mass might lead to the same effect as the energy dependence of the relaxation time.[25] In this work, we account for the overall influence of band non-parabolicity through temperature dependence of carrier effective mass.[9]

We employ the following expression for the Fermi level for an n-type semiconductor with completely ionised donors in the temperature range over which the Boltzmann distribution function can be used[26]

$$E_{\mathrm{F}}(T) = \frac{1}{2}(E_v + E_c) + \frac{3}{4}k_{\mathrm{B}}T\ln\left(\frac{m_p^*}{m_n^*}\right)$$
$$+ k_{\mathrm{B}}T\sinh^{-1}\left(\frac{N_d}{2\sqrt{U_c U_v}\exp(-\zeta_g)}\right). \qquad (12)$$

Here, E_v and E_c are the energies of the valence and conduction band edges, m_n^* and m_p^* are the density-of-states effective masses for the conduction and valence bands, N_d is the concentration of ionised donors, $U_{c(v)} = 2(2\pi m_{n(p)}^* k_{\mathrm{B}}T/h^2)^{3/2}$, and $\zeta_g = (E_c - E_v)/k_{\mathrm{B}}T$ is the reduced band gap.

Following Drabble and Goldsmid,[20] we express the electronic conductivity ρ^{-1}, Seebeck coefficient S, and the monopolar electron thermal conductivity κ_{mp} as follows:

$$\rho^{-1} = \frac{2\hbar e^2 \varrho\, c_l^2}{3\pi \Xi^2 m_n^*}\,F_0(\zeta), \qquad (13)$$

$$S = -\frac{k_{\mathrm{B}}}{e}\left[\zeta - \frac{2F_1(\zeta)}{F_0(\zeta)}\right], \qquad (14)$$

$$\kappa_{\mathrm{mp}} = \left(\frac{k_{\mathrm{B}}}{e}\right)^2\left[\frac{3F_2(\zeta)}{F_0(\zeta)} - \left(\frac{2F_1(\zeta)}{F_0(\zeta)}\right)^2\right]\rho^{-1}T, \qquad (15)$$

where e is the magnitude of electronic charge, Ξ is the deformation potential, ϱ is the density, $\zeta = E_{\mathrm{F}}/k_{\mathrm{B}}T$ is reduced Fermi energy, and F_n is the Fermi integral

$$F_n(\zeta) = \int \frac{x^n dx}{\exp(x-\zeta)+1}. \qquad (16)$$

As the temperature rises, the electronic thermal conductivity will have an added contribution from the bipolar

(electron-hole pair) component κ_{bp}, which is calculated using the expression[27]

$$\kappa_{\mathrm{bp}} = \frac{b}{(b+1)^2}\left[\zeta_g + 4\right]^2\left(\frac{k_B}{e}\right)^2\rho^{-1}T, \qquad (17)$$

where b is the carrier mobility ratio $\mu_{\mathrm{n}}/\mu_{\mathrm{p}}$ and E_g is the electronic band gap. In the intrinsic temperature range, the electronic conductivity can be written as[26]

$$\rho_{int}^{-1} = 2e\left(\frac{k_{\mathrm{B}}T}{2\pi\hbar^2}\right)^{3/2}(m_n^* m_p^*)^{3/4}(\mu_n + \mu_p)e^{-\zeta_g/2}. \qquad (18)$$

PbTe is highly ionic, with the ionicity factor of 0.63 on the Phillips scale. Following the suggestion in Ref. 28 that the temperature dependence of the mobility of ionic semiconductors is predicted to be proportional to $T^{-1/2}$, we may then express Eq. (18) in the form

$$\rho_{int}^{-1} = DTe^{-\zeta_g/2}, \qquad (19)$$

where D is an appropriate constant.

III. RESULTS

For phonon calculations, we used $q_{\mathrm{D}} = 0.908 \times 10^{10}\,\mathrm{m}^{-1}$, $c_{\mathrm{TA}} = 1038\,\mathrm{m/s}$, $c_{\mathrm{LA}} = 1633\,\mathrm{m/s}$, $c_{\mathrm{TO}} = 1175\,\mathrm{m/s}$, and $c_{\mathrm{LO}} = 1073\,\mathrm{m/s}$. The phonon anharmonic interaction was treated by considering the Grüneisen constant γ as an adjustable parameter. It was found that $|\gamma| = 0.8$ (resulting in the value $(\gamma/\bar{c})^2 = 4.9 \times 10^{-11}\,\mathrm{s}^{-2}\mathrm{cm}^{-2}$) was a good choice for explaining the high temperature conductivity results for all the three samples. We note that our semi-adjustable choice for γ is lower than the thermodynamically deduced estimate of approximately 1.4 reported in the work by Ravich et al.[9] and the theoretically calculated acoustic-phonon value of 2.18.[29] The electronic parameters used in this study are carrier concentration $n = 2.6 \times 10^{18}\,\mathrm{cm}^{-3}$, material mass density $\varrho = 8.242 \times 10^3\,\mathrm{kg/m^3}$, deformation potential $\Xi = 4.5\,\mathrm{eV}$, electron effective mass $m^* = 0.41m_0$ (m_0 being electron mass), and electronic band gap $E_g = 0.38\,\mathrm{eV}$. Our choice for the deformation potential is somewhat smaller than that reported in the Monte Carlo simulation by Palankovski et al.[30]

A. Vibrational and thermal properties

1. Phonon dispersion curves and density of states

Our modelled phonon linear dispersion relations and the corresponding density of states are shown in Fig. 1. The choices for the Debye radius q_{D} and the branch speeds c_s listed earlier were made to obtain reasonable agreement with the neutron scattering data and a theoretical modelling for the dispersion curves and the density of states presented by Cochran et al.[31] Our computed density of states curve also shows reasonably good agreement with first-principle results obtained in Refs. 29 and 32. It is interesting to note that the doubly degenerate TO is a low-lying branch and its slope is comparable to that of the doubly-degenerate TA branch.
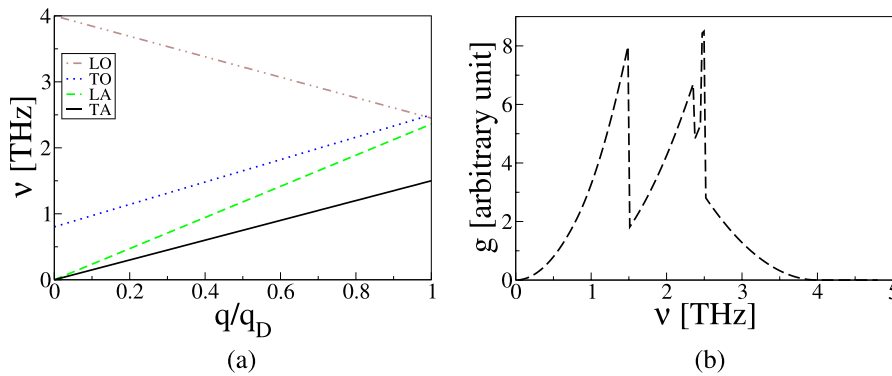
FIG. 1. (a) Linearised phonon dispersion relations in PbTe and (b) the corresponding density of states.

2. Lattice specific heat

The calculated results for the specific heat at constant volume (C_v) agree very well with experimental measurements[33] in the low temperature range up to 50 K, as seen in Fig. 2. This vindicates the application of the present continuum theory. Above this temperature, our theoretical results are underestimated when compared with the experimental results as well as the *ab inito* results from Zhang *et al.*[29] and Bencherif *et al.*[32] We believe that the use of accurate phonon dispersion curves, together with a realistic Brillouin zone summation technique, would improve agreement between theory and experiment. We tested this hypothesis by repeating our calculations with different slopes of the LO branch. It was found that changing the LO speed from 1073 m/s to 1400 m/s resulted in an increase of 5% in C_v at 300 K.

However, the *ab-initio* work by Zhang *et al.*[29] obtains results that are higher than experiment at low temperatures (below 25 K) and the *ab-initio* study by Bencherif *et al.*[32] has obtained results that are lower than experimental results at high temperatures. These studies did not offer any explanation for these discrepancies. We made a comparative study of these *ab-initio* results from the two groups, by plotting their results together in Fig. 2, and found that rather large uncertainty may be expected in computing C_v from such techniques. Thus, we cannot be sure of the exact reason for the discrepancy between theory and experiment for C_v and suggest that further theoretical and experimental studies are necessary to resolve the issue.

The underestimation of our theoretical C_v values at high temperatures should not affect our intended study of the lattice thermal conductivity. This is because our formalism of the conductivity requires unavoidable use of adjustable parameters for phonon-defect and phonon-phonon scattering mechanisms, as described in the next section.

3. Lattice thermal conductivity

Figure 3(a) shows two separate calculations of the conductivity for the sample from Ref. 6: the black solid curve represents results by considering acoustic phonons as heat carriers but including their interaction with optical phonons, and the green dashed-dotted curve represents the results when both acoustic as well as optical phonons are considered as heat carriers and allowed anharmonic interactions among all branches are included. The lattice thermal conductivity at room temperature is found to be $\sim$1.1 W m^{-1} K^{-1} when optical phonons are not considered to transfer heat but are allowed to interact with acoustic phonons. The lattice thermal conductivity increases to $\sim$1.5 W m^{-1} K^{-1} at room temperature when all phonon modes participate in conducting heat with a full range interaction between acoustic and optical phonons dictated by the momentum and energy conservation conditions. It is clear that the optical phonon modes do indeed contribute significantly to the lattice thermal conductivity in PbTe. We note, however, that the difference between acoustic alone (κ_{ph} (ac)) and acoustic + optical (κ_{ph} (ac+op)) is not a simple constant. As seen from Fig. 3(b), the percentage contribution from the acoustic phonons slightly decreases with increase in temperature: being 56% at 300 K and 53% at 800 K. In Fig. 3(c), we have broken the lattice thermal conductivity into its components. We notice that the TA and TO branches contribute, respectively, up to 43% and 38% of the total thermal conductivity at room temperature. As the temperature increases, the contribution of the TO branch becomes a little larger than the contribution of the TA branch.

Recently, Tian *et al.*[34] have made *ab initio* calculations of the lattice thermal conductivity of PbTe in the limited temperature range of 300–700 K. Our results in general agree with their results. Both works conclude that the optical phonons in this material play an important role in heat conduction. In agreement with our work, Tian *et al.* conclude, by accounting for all acoustic and optical branches, that the omission of ac-op scattering increases the conductivity by
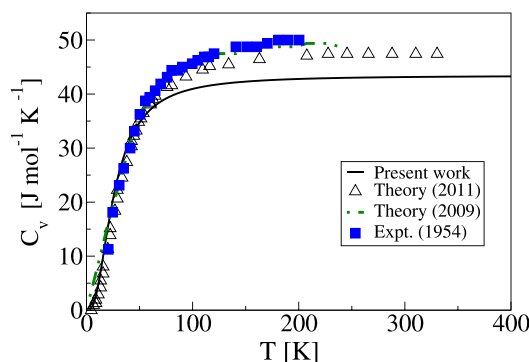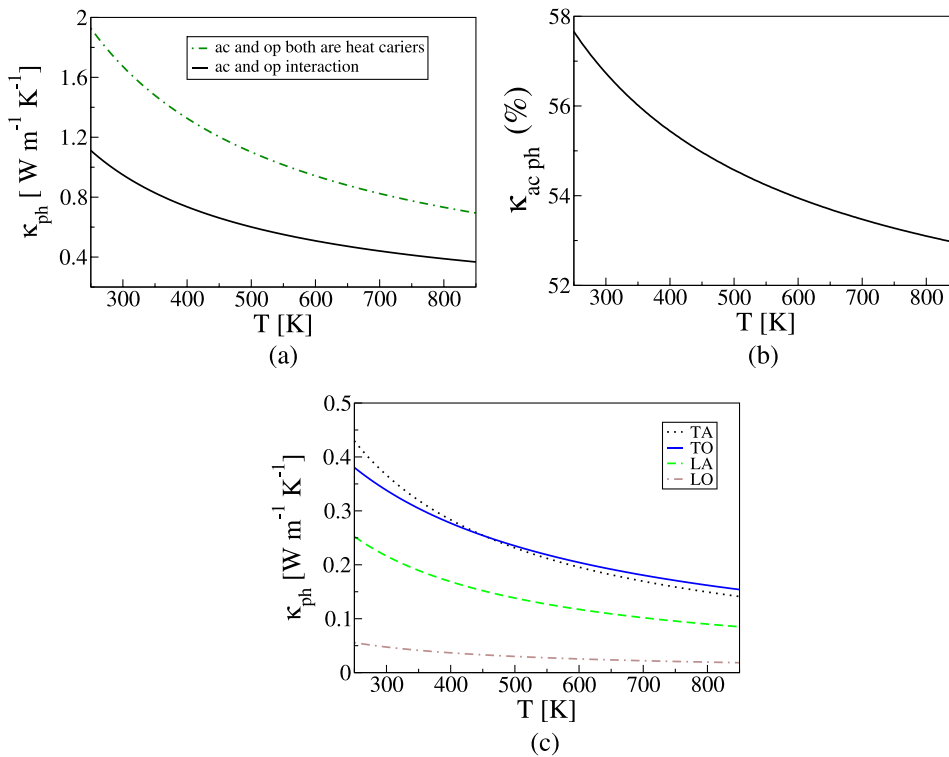

FIG. 2. Lattice specific heat at constant volume C_v for PbTe. The results from the present work are compared with the experimental measurements (Experiment (1954)[33]) and first-principles theoretical calculations (Theory (2009)[29] and Theory (2011)[32]).

(a)

(b)

(c)

FIG. 3. Calculated lattice thermal conductivity κ_{ph} results for sample 1. In panel (a), the black solid curve represents the results by considering the acoustic phonons as heat carriers but including their interaction with optical phonons, and the green dashed-dotted curve represents the results when both acoustic as well as optical phonons are considered as heat carriers and allowed anharmonic interactions among all branches are included. Panel (b) shows the percentage contribution from acoustic phonons. Panel (c) shows contributions from individual acoustic and optical branches.

roughly a factor of five. Our work also agrees with Tian *et al.* in that the LO phonons make the lowest contribution and the TA phonons contribute at the highest end. However, our work differs with Tian *et al.* with respect to the contributions from the LA and TO phonons. While Tian *et al.* find that LA phonons contribute much more than TO phonons, our work suggests that the TO contribution is approximately 10% larger than the LA contribution.

It would not be inappropriate to comment that Zhang *et al.*[29] reported two different results (1.66 and 2.01 W m^{-1} K^{-1}) for the room-temperature lattice thermal conductivity of PbTe using two differently calculated (and much larger) values of the acoustic-phonon Grüneisen constant (2.18 and 1.96, respectively). Although their results are quite similar to the results presented in this work and the experimental results in Fig. 4, it should be emphasized that these authors used a grossly simplified expression for phonon anharmonic interaction and did not take into account any other form of phonon interaction (such as defect scattering).
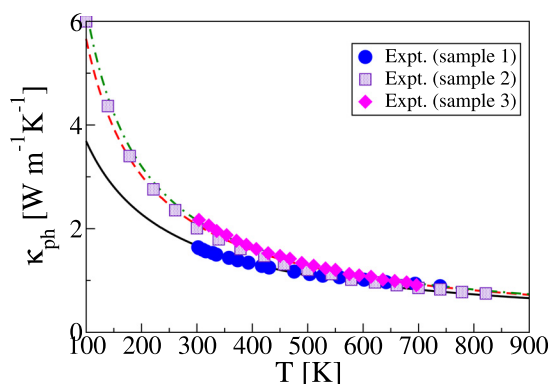
In Fig. 4, we present our computed results for the lattice thermal conductivity κ_{ph} for three samples of PbTe, in the temperature range 100–900 K. Our results are validated against several experimental results taken from Ref. 6 (sample 1), Ref. 9 (sample 2) and Ref. 35 (sample 3), both for the magnitude and the temperature variation. Experimental measurements are available in the temperature ranges 300–750 K for sample 1, 100–800 K for sample 2, and 300–700 K for sample 3. The results for samples 2 are slightly lower than that for sample 3 in the common temperature range these have been presented. The results for sample 1 fall lower than those for samples 2 and 3 below 500 K, indicating that it is more defective. In order to reproduce the experimental data for these n-type samples, we had to adjust the boundary length and the point defect concentration. The values of the effective boundary length and the adjusted point defect parameter are given in Table I. As shown in the table, in order to fit the experimental data for samples 2 and 1 we had to use almost twice and ten times the point-defect scattering rate compared to that for sample 3. The agreement between theory and experiment was refined by choosing slightly different boundary lengths for the three samples, as presented in the table.

FIG. 4. Lattice thermal conductivity results (κ_{ph}) for three different n-PbTe samples taken from Refs. 6 (sample 1), 9 (sample 2), and 35 (sample 3).

TABLE I. Effective boundary length L and adjusted point defect parameter B_{pd} used for fitting the experimental results of lattice thermal conductivity for three samples of PbTe.

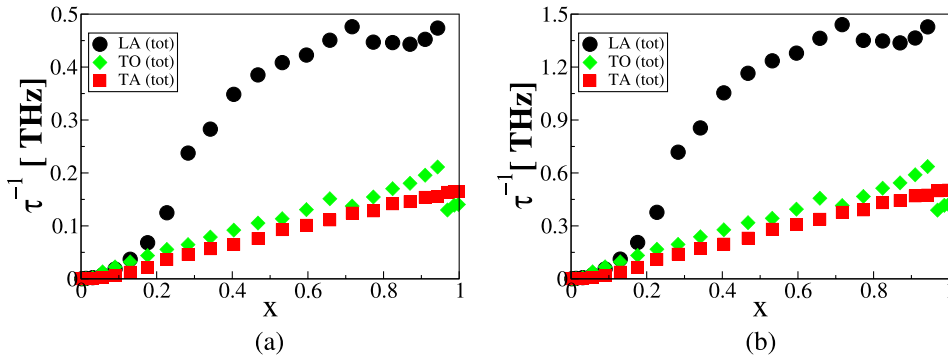| Sample Ref.	Effective boundary length L (μm)	Point defect parameter A_{pd} (s^3)
Sample 1 (Ref. 6)	0.34	1.039×10^{-41}
Sample 2 (Ref. 9)	0.50	2.078×10^{-42}
Sample 3 (Ref. 35)	0.05	1.039×10^{-42}

FIG. 5. The total anharmonic relaxation rate for LA, TA, and TO branches as a function of the reduced wave vector at (a) T = 300 K, (b) T = 900 K for PbTe.

a. Total anharmonic relaxation rates. In order to emphasise the relative importance of different phonon branches towards the thermal conductivity, we plot the inverse anharmonic relaxation times of phonons as a function of the reduced wave number in Figs. 5(a) and 5(b). For all wave numbers, τ^{-1}(LA) is much larger than τ^{-1}(TA) and τ^{-1}(TO). Also, for all wave numbers τ^{-1}(TO) is $\sim \tau^{-1}$(TA) at both low and high temperatures. Figures 5(a) and 5(b) also demonstrate that in the low frequency range the relaxation rate for the LA branch follows the ω^2 behaviour, as predicted by Klemens,[36] whereas the TO and TA branches show a mixture of linear and quadratic behaviours. As the reduced wave number increases, the behaviour of τ_{LA}^{-1} in general shows a polynomial type dependence on ω. This analysis is in good agreement with the trend noted by Tian *et al.*[34]

b. Normal anharmonic relaxation rates involving different polarisations and branches. Normal anharmonic relaxation rates for several class 1 processes $s + s' \rightarrow s''$ involving different phonon polarisations and branches are presented in Fig. 6. A few observations can be made. The scattering rates

for the processes involving only acoustic phonons (i.e., $ac + ac \rightarrow ac$) or only optical phonons (i.e., $op + op \rightarrow op$) are the weakest, as seen form the results in panels (a) and (d). The results in panels (b) and (c) indicate that the strongest $ac + op \rightarrow op$ interactions involve TA and TO phonons merging together to produce LO phonons. Normal (N) processes are not allowed for certain range of x values, due to the demand of simultaneous momentum and energy conservation considerations. This is very clearly seen in panel (d), which suggests that the process $TO + TO \rightarrow LO$ is not allowed for $x < 0.1$ and for $x > 0.7$. It is also found that the maximum strengths for the processes $TO + TA \rightarrow TO$ (N) and $TO + LA \rightarrow LO$ (N) are almost similar, except that the former (latter) is more effective for shorter (longer) wave numbers.

c. Comparison between N and U relaxation rates. The results presented in Fig. 7 compare the N and U relaxation rates for two (randomly chosen) processes. Both for $LA + TA \rightarrow LA$ and $TA + TA \rightarrow TO$, the N process is stronger than the U process for almost all wave numbers of the

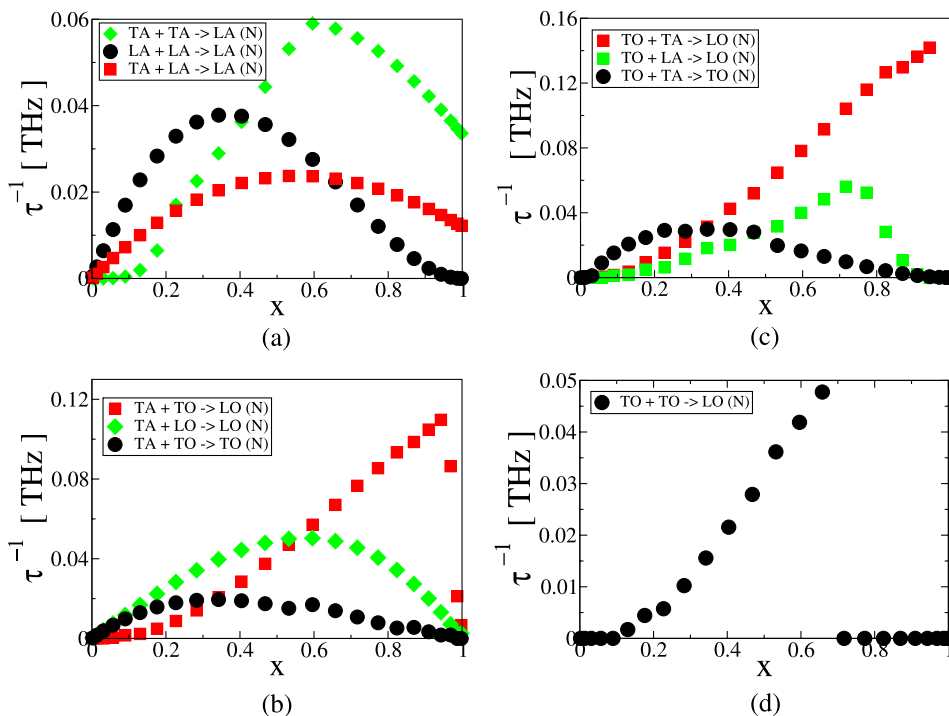

FIG. 6. Anharmonic scattering rates at T = 900 K for (a) $ac + ac \rightarrow ac$ (N), (b) $ac + op \rightarrow op$ (N), (c) $op + ac \rightarrow op$ (N), and (d) $op + op \rightarrow op$ (N) processes.
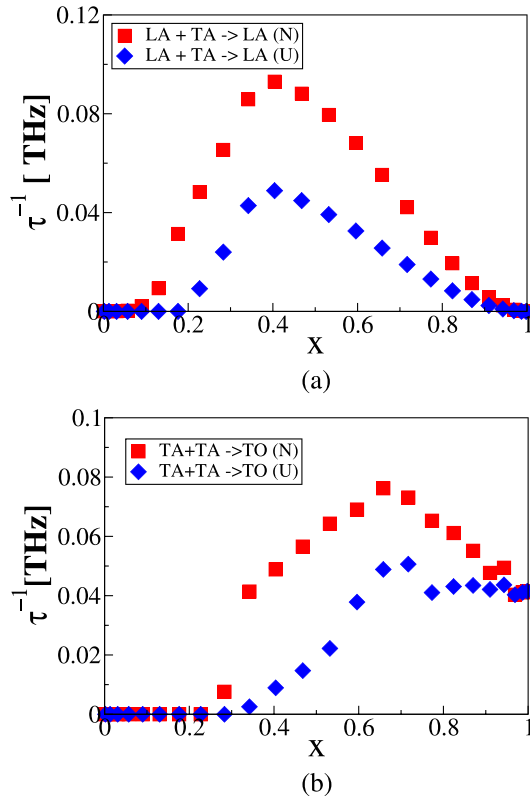
FIG. 7. Comparison between N and U scattering rates at T = 900 K for the relaxation of LA and TA phonons.

relaxing phonon (indicated as s in the process $s + s' \rightarrow s''$). Only when the wave number gets closer to the Debye radius (typically when $x = 0.9$) does the U process become comparable to the N process. Such a comparison between N and U processes has been noted before.[37]

We also mention that the results in Figs. 6(a) and 7(a) further suggest that the relaxation rate of LA phonons via the process LA + TA → LA (N) is approximately three times stronger than that of TA phonons via the process TA + LA → LA (N).

d. Frequency and temperature dependence of anharmonic relaxation rate. The total three-phonon Normal scattering rate and the total relaxation rate for the TO and TA phonons, at a given reduced wave number, as a function of low temperatures, are shown in Fig. 8(a). The dependences of $\tau^{-1}_{TO,TA}$ are not linear in the low temperatures range, with $\tau^{-1}_{TO} > \tau^{-1}_{TA}$. The latter can be explained by noticing that for a given q, $\omega_{TO} > \omega_{TA}$ and that at low temperatures $\tau^{-1}(\omega,T) \propto \omega^n T^{5-n}$.[38] As the temperature increases beyond 100 K, the scattering rates change linearly with T. In fact, the linearity behaviour starts earlier than 100 K for the TA mode, which may be attributed to a low TA Debye temperature. Panel (c) offers a comparison between the relaxation rates for the TO and TA modes at a high reduced wave number $x = 0.969$, where it is noted that at a given temperature the scattering rate of TO is much weaker than that of TA. Our work provides support to the previous suggestion[14] that the TO phonons are involved in strong anharmonic interactions. However, although the work in Ref. 14 has identified strong TO–LA interaction, our work suggests that TO–TA interaction is stronger.
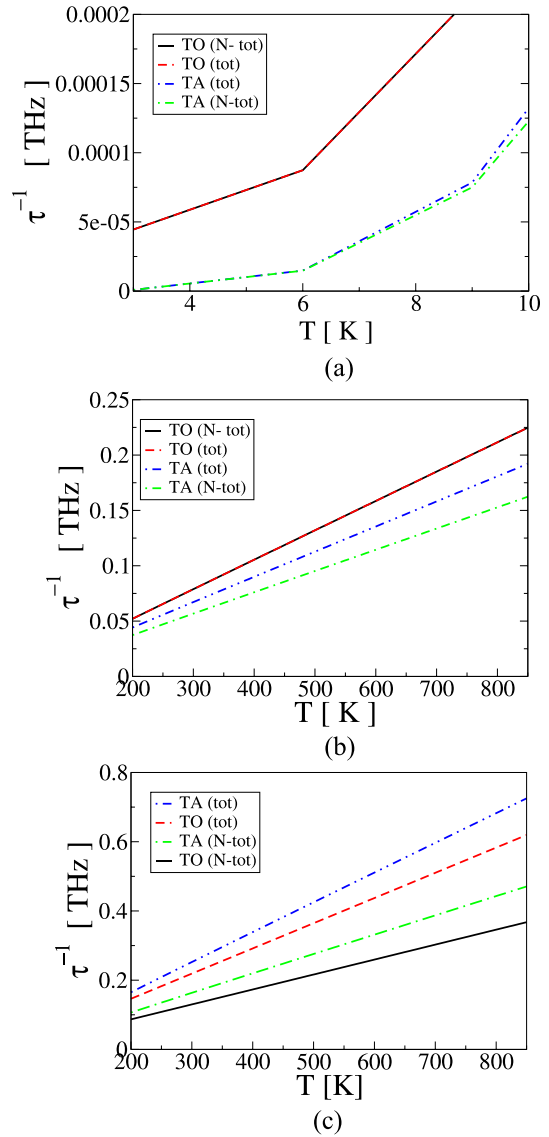

FIG. 8. Relaxation rates of the total Normal processes and the total anharmonic processes for TO and TA phonons at $x = 0.342$ for (a) low temperatures and (b) high temperatures. Panel (c) presents the relaxation rate of the total Normal processes and the total anharmonic processes for TO and TA phonons at $x = 0.969$ as a function of temperature.

B. Electronic transport coefficients

Figure 9 shows the temperature variation of Fermi level in the n-PbTe sample studied in this work. With increase in temperature, the level decreases below the conduction band minimum as more and more donors get ionised. Approximately above 650 K, the donors are all ionised, and the temperature variation of Fermi level becomes that of the intrinsic nature.

Figure 10(a) shows the temperature variation of the Seebeck coefficient S. The magnitude $|S|$ increases as the temperature increases and shows a turning point at about 650 K due to the intrinsic excitation through this narrow band semiconductor at high temperatures, where holes as well as electrons make contribution. Our computed results are in good agreement with the experimental data from Ref. 6. As usually Fermi level is extracted from measurements of the Seebeck coefficient, it is pleasing to remark that Eq. (12)
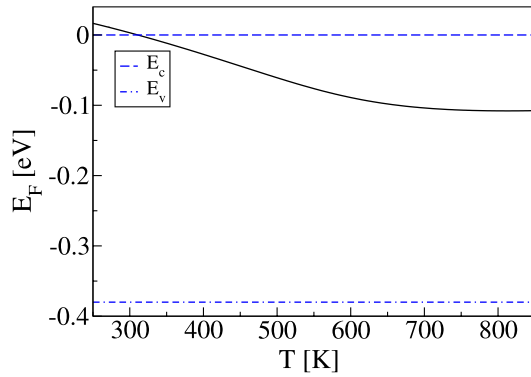
FIG. 9. Temperature variation of Fermi level in n-type PbTe with donor concentration $2.6 \times 10^{18}\,cm^{-3}$. The conduction band and valence band edges are drawn as dashed and dashed-dotted horizontal lines, respectively.

presents a reliable simple analytical expression for the temperature variation of Fermi level in n-type PbTe.

The influence of band non-parabolicity on acoustic phonon scattering is taken into account through the effective mass temperature dependence.[9] This dependence is reported in Ref. [39] to be of the order $\propto T^{0.5}$ for electrons and accordingly we used $m_n^*(0) = 0.02\,m_0$ for this calculation. The large non-parabolicity for PbTe in its lowest conduction band, combined with its narrow gap characteristic, is considered to be the cause of this significant temperature dependence of the effective mass, which also can be explained by a thermal distribution of electrons over non-parabolic band.[25] Furthermore, as suggested by Moyzhes and Ravich in Ref. [10], we expect the energy dependence of the relaxation time for acoustic scattering to deviate from the 1/2 power law as a consequence of non-parabolicity. Figure 10(b) shows the results for the electrical resistivity ρ. With consideration of electron scattering with acoustic phonons alone, the results for the extrinsic contribution show reasonable agreement up to 600 K with the experimental data presented in Ref. [6]. At higher temperatures, when the specimen can be assumed to be intrinsic, the results shown in Fig. 10(b) for the intrinsic resistivity are obtained by treating the dependence of the effective mass, mobility, and the variation of energy gap that appears in Eq. (18) by fitting the constant $D = 0.794\,\Omega\,cm$.[40] There is very good agreement between the computed extrinsic contribution and the experimental data at temperatures above 700 K. On the whole, we regard the agreement between our theoretical results and the experimental data as reasonable.

With the electrical resistivity ρ computed, the electronic contribution to the thermal conductivity was computed by using the Wiedemann-Franz relationship. In particular, in the extrinsic regime, κ_{mp} was computed using Eq. (15) and in the intrinsic regime κ_{bp} was computed using Eq. (17).

C. Total thermal conductivity

The total thermal conductivity is expressed as

$$\kappa_{tot} = \kappa_{el} + \kappa_{ph}, \tag{20}$$

where κ_{el} is the contribution from the carriers (donor electrons (monopolar) in the extrinsic regime and electron-hole
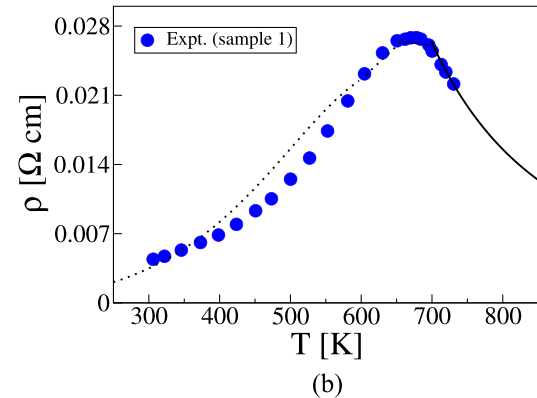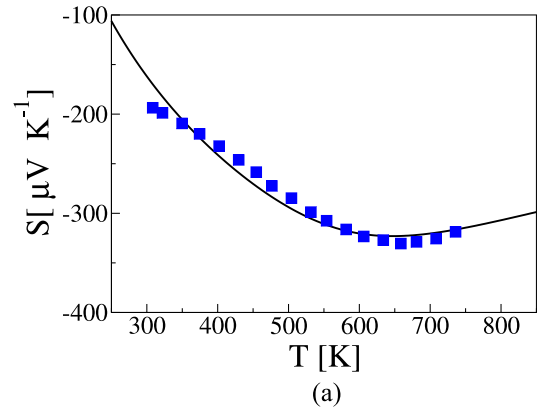

FIG. 10. (a) Seebeck coefficient and (b) electrical resistivity for the n-type PbTe with donor concentration $2.6 \times 10^{18}\,cm^{-3}$. The solid and dot curves for ρ represent the intrinsic (monopolar) and extrinsic (bipolar) contributions, respectively. The experimental data are read from Ref. [6].

pairs (bipolar) in the intrinsic regime, and κ_{ph} is the phonon conductivity. Our computed results for sample 1 are compared with the experimental results reported by Pei and Liu[6] in Fig. 11. There is very good agreement between theory and experiment. Considerable decrease in the conductivity is noted as the temperature increases: for example, from 1.7 W K^{-1} m^{-1} at room temperature to 1.1 W K^{-1} m^{-1} at 650 K. The upward change in the slope of the κ–T curve above 500 K is due to the electronic contribution (largely to the bipolar contribution).

D. Thermoelectric figure of merit

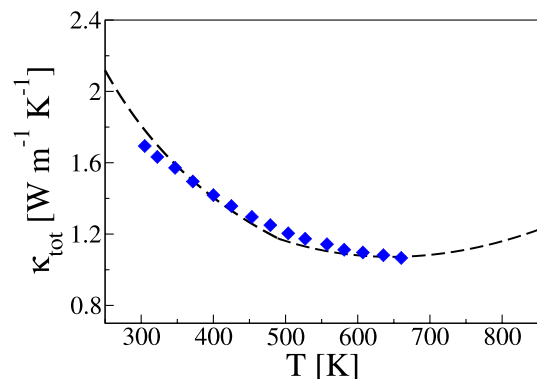The temperature variation of the dimensionless figure of merit ZT is presented in Fig. 12 for two scenarios of the

FIG. 11. Total thermal conductivity ($\kappa_{tot} = \kappa_{el} + \kappa_{ph}$) of sample 1.[6]
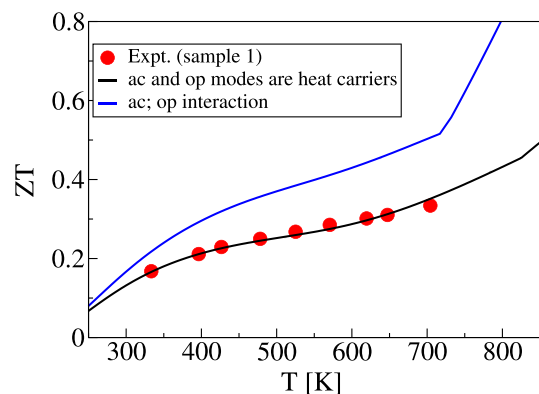
FIG. 12. Figure of merit ZT for the n-type sample of PbTe prepared and studied by Pei *et al.*[6] The experimental data is deduced from the measured values of S, ρ and κ_{tot} in Ref. 6).

lattice thermal conductivity: (i) by considering only acoustic phonons as heat carriers (but incorporating the ac-op interactions), and by (ii) considering acoustic as well as optical phonons as heat carriers (and incorporating all allowed interactions among the acoustic and optical phonons). The larger figure of merit is achieved when optical phonons are not considered as heat carriers (i.e., for scenario (i)). The room-temperature result for the figure of merit ZT increases from 0.1 for scenario (ii) to 0.17 for scenario (i). This clearly indicates the important role played by the existence of the low-lying TO branch in PbTe.

While our theoretical work reproduces the experimentally obtained data for S, ρ, and $\kappa_{tot} = \kappa_{el} + \kappa_{ph}$, we did not manage to match our calculated ZT values with the results in Ref. 6. However, our results of the figure of merit ZT, with the contribution to the lattice thermal conductivity by all branches considered, are consistent with the values extracted directly from the measurements of S, ρ, and κ_{tot} reported in Ref. 6. It appears, therefore, that there are numerical errors in the ZT values presented in Ref. 6. This has been confirmed[41] by one of the authors of Ref. 6.

IV. SUMMARY

By employing the nearly-free-electron theory and a single non-parabolic electronic band, and a continuum theory of harmonic and anharmonic phonons for all acoustic and optical branches, we have successfully reproduced the experimental measurements of all the thermoelectric transport coefficients for an n-type sample of PbTe. The results presented here show that the band non-parabolicity influences the electronic transport coefficients via a temperature-dependent effective mass temperature. The TO phonons make a significant contribution to the lattice thermal conductivity and are found to play an important role in determining the figure of merit ZT. The strongest anharmonic interaction is predicted to arise from the Normal (N) TO + TA → LO process. The total anharmonic relaxation rate of the TO phonons is quite similar to that of the TA phonons but much smaller than that of the LA phonons. It can be assumed that the suppression, or reduction, of the contribution of the TO branch, by an appropriate addition of

scattering processes would enhance the thermoelectric properties of PbTe and increase the figure of merit considerably.

[1]D. M. Rowe, *CRC Handbook of Thermoelectrics* (CRC Press, New York, 1995).
[2]H. J. Goldsmid, *Introduction to Thermoelectricity* (Springer, 2010).
[3]Y. Pei *et al.*, Energy Environ. Sci. **4**, 2085 (2011).
[4]A. D. Lalonde, Y. Pei, and G. J. Snyder, Energy Environ. Sci. **4**, 2090 (2011).
[5]D. Greig, Phys. Rev. **120**, 358 (1960).
[6]Y.-L. Pei and Y. Liu, J. Alloys Compd. **514**, 40 (2012).
[7]T. S. Stavyzkay, L. V. Prokophye, Yu. I. Ravich, and B. A. Efimova, Fiz. Tech. Pol. **1**, 1138 (1967).
[8]I. A. Smyrnoff and Yu. I. Ravich, Fiz. Tech. Pol. **1**, 891 (1967).
[9]Yu. I. Ravich, B. A. Efimova, and I. A. Smirnov, *Semiconducting Lead Chalcogenides* (Plenum Press 1970), p. 89.
[10]B. Ya. Moyzhes and Yu. I. Ravich, Fiz. Tech. Pol. **1**, 188 (1967).
[11]C. Wood, Rep. Prog. Phys. **51**, 459 (1988).
[12]G. S. Nolas, J. Sharp, and H. J. Goldsmid, *Thermoelectrics, Basic Principles and New Materials Developments* (Springer, 2001).
[13]J. P. Heremans, V. Jovovic, E. S. Toberer, A. Saramat, A. Charoenphakdee, Shi. Yamanaka, and G. J. Snyder, Science **321**, 554 (2008).
[14]O. Delaire, J. Ma, K. Marty, A. F. May, M. A. McGuire, M. H. Du, D. J. Singh, A. Podlesnyak, G. Ehlers, M. D. Lumsden, and B. C. Sales, Nature Mater. **10**, 614 (2011).
[15]G. P. Srivastava, *The Physics of Phonons* (Adam Hilger, Bristol, 1990).
[16]P. Carruthers, Rev. Mod. Phys. **33**, 92 (1961).
[17]J. M. Ziman, Philos. Mag. **1**, 191 (1956); **2**, 292 (1957).
[18]J. E. Parrott, Proc. Phys. Soc. **81**, 726 (1963).
[19]R. A. H. Hamilton and J. E. Parrott, Phys. Rev. **178**, 1284 (1969).
[20]J. R. Drabble and H. J. Goldsmid, *Thermal Conduction in Semiconductors* (Pergamon Press 1961), p. 108.
[21]D. M. Zayachuck, Phys. Tech. Semicond. (Russia) **31**, 217 (1997).
[22]Yu. I. Ravich, B. A. Efimova, and V. I. Tamarchenko, Phys. Status Solidi B **43**, 11 (1971).
[23]W. Zawadsky, "Electron transport phenomena in small gap semiconductor," Adv. Phys. **23**, 435 (1974).
[24]D. M. Freik, L. I. Nykyruy, and V. M. Shperun, Semicond. Phys. Quantum Electron. Optoelectron. **5**, 362 (2002).
[25]Yu. I. Ravich, J. Phys. Colloq. **29**, C4 (1968).
[26]J. P. McKelvey, *Solid State and Semiconductor Physics*, International ed. (Harper and Row, New York).
[27]P. J. Price, Philos. Mag. **46**, 1252 (1955).
[28]A. F. Ioffe, *Physics of Semiconductors* (Infosearch Ltd., 1960).
[29]Y. Zhang, X. Ke, C. Chen, J. Yang, and P. R. C. Kent, Phys. Rev. B **80**, 024304 (2009).
[30]V. Palankovski, M. Wagner, and W. Heiss, *Springer Proceedings in Physics* (Springer, Dordrecht, 2008), Vol. 119, p. 77.
[31]W. Cochran, R. A. Cowley, G. Dolling, and M. M. Elcombe, Proc. R. Soc. London, Ser. A **293**, 433 (1966).
[32]Y. Bencherif, A. Boukra, A. Zaoui, and M. Ferhat, Infrared Phys. Technol. **54**, 39 (2011).
[33]D. H. Parkinson and J. E. Quarrington, Proc. Phys. Soc. **67**, 569 (1954).
[34]Z. Tian, J. Garg, K. Esfarjani, T. Shiga, J. Shiomi, and G. Chen, Phys. Rev. B **85**, 184303 (2012).
[35]J. R. Sootsman, R. J. Pcionek, H. Kong, C. Uher, and M. G. Kanatzidis, Chem. Mater. **18**, 4993 (2006).
[36]P. G. Klemens, Proc. R. Soc. London, Ser. A **208**, 108 (1951).
[37]G. P. Srivastava, Pramāna **6**, 1 (1976).
[38]C. Herring, Phys. Rev. **95**, 954 (1954).
[39]H. A. Lyden, Phys. Rev. **135**, A514 (1964).
[40]E. Miller, K. Komarek, and I. Cadoff, J. Appl. Phys. **32**, 2457 (1961).
[41]One of the authors of Ref. 6 was contacted regarding the difference between their presented experimental data for S and σ and their computed maximum of ZT. They have confirmed the inconsistency in their graphs, indicating that their corrected ZT results are consistent with ours.